



Observation of the Hydrogen-Dislocation Interactions in a High-Manganese Steel after Hydrogen Adsorption and Desorption

Dayong An¹ · Yuhao Zhou² · Yao Xiao² · Xinxi Liu¹ · Xifeng Li¹ · Jun Chen¹

Received: 8 March 2022 / Revised: 22 April 2022 / Accepted: 24 April 2022 / Published online: 6 June 2022
© The Chinese Society for Metals (CSM) and Springer-Verlag GmbH Germany, part of Springer Nature 2022

Abstract

Hydrogen embrittlement (HE) poses a significant challenge for the development of high-strength metallic materials. However, explanations for the observed HE phenomena are still under debate. To shed light on this issue, here we investigated the hydrogen-defect interaction by comparing the dislocation structure evolution after hydrogen adsorption and desorption in a Fe-28Mn-0.3C (wt%) twinning-induced plasticity steel with an austenitic structure using in situ electron channeling contrast imaging. The results indicate that hydrogen can strongly affect dislocation activities. In detail, hydrogen can promote the formation of stacking faults with a long dissociation distance. Besides, dislocation movements are frequently observed during hydrogen desorption. The required resolved shear stress is considered to be the residual stresses rendered by hydrogen segregation. Furthermore, the microstructural heterogeneity could lead to the discrepancy of dislocation activities even within the same materials.

Keywords Hydrogen embrittlement · Stacking fault · Dislocation movement · High-manganese steel · Electron channeling contrast imaging (ECCI)

1 Introduction

High-strength metallic materials, e.g., high-manganese steel (HMnS), always suffer unexpected catastrophic failure when they are exposed to a hydrogen-rich environment [1, 2], which is known as hydrogen embrittlement (HE). Although the HE problem has been identified for more than one century, it is still one of the major industrial challenges, particularly for the development of advanced structural materials [3]. Due to the very small H atomic radius, absorption and diffusion of hydrogen atoms in metals can occur at ambient temperature [4]. As a result, the mechanical properties of high-strength metals could be dramatically degraded by the

interaction between solute H and defects (e.g., grain boundaries (GBs), dislocations, and vacancies) even when the H uptake is extremely low (parts per million, ppm) [5, 6].

To explain the HE phenomenon, a series of H-microstructure interaction mechanisms have been proposed. The hydrogen-enhanced localized plasticity (HELP) mechanism claims that the hydrogen atmospheres can shield the dislocation stress fields and, thus, reduce the interactions between dislocations and obstacles [7]. Consequently, hydrogen enhances the local dislocation activity and facilitates the formation of cracks. Through in situ environmental transmission electron microscopy (TEM) experiments, Robertson et al. [8] found that two HE mechanisms were associated in Ti-4Al (wt%) alloy: one is fracture by localized plastic deformation enhanced by hydrogen, and the other is the brittle fracture of the stress-induced precipitation of hydrides. The HELP mechanism was further supported by the enhanced dislocation pile-ups in 310S stainless steel [9] and the change in the stress field of the dislocation-hydrogen complex obtained by combining experimental and numerical methods [10]. Another intensely discussed HE mechanism, named hydrogen-enhanced decohesion (HEDE) [11], proposes that the accumulated hydrogen atoms near crack tips weaken the interatomic cohesive forces and therefore can reduce the

Dayong An, Yuhao Zhou have contributed equally to this work.

Available online at <http://link.springer.com/journal/40195>.

✉ Dayong An
d.an@sjtu.edu.cn

¹ Department of Plasticity Technology, School of Materials Science and Engineering, Shanghai Jiao Tong University, Shanghai 200030, China

² State Key Laboratory of Solidification Processing, Northwestern Polytechnical University, Xi'an 710072, China

fracture energy. Besides, Kirchheim et al. [12] came up with the defactant concept, claiming that hydrogen can reduce the formation energy of defects. Hermida et al. [13] reported that the formation of hydrogen pairs could reduce the stacking fault energy (SFE) of austenitic stainless steel. Koyama et al. [14] investigated the HE of a Fe-18Mn-1.2C (in wt%) steel by using electron channeling contrast imaging (ECCI). The results revealed that deformation twins were also preferred nucleation sites of hydrogen-assisted cracks. Lu et al. [15] investigated the effect of hydrogen on the deformation behavior of a HMnS using an in situ micropillar compression test and found that hydrogen promoted both dislocation multiplication and twin formation. In a previous study [16], we found that hydrogen would assist the nucleation of stacking fault (SF) and formation of deformation-induced martensite in a Fe-27.81Mn-0.3C (in wt%) twinning-induced plasticity (TWIP) steel.

Although numerous HE mechanisms have been proposed, the specific origins of HE for different materials and microstructures are still under debate [17]. This can be ascribed to several aspects. First, HE susceptibility is affected by many factors. For example, Wang et al. [18] found that the fracture stress of high-strength steel decreased with increasing diffusible hydrogen concentration. Besides, the chemical composition can also affect the HE susceptibility in terms of changing its phase stability [19]. Moreover, various underlying processes proposed by different HE mechanisms may lead to similar morphological features on the fracture surfaces [17]. In addition, it is still extremely challenging to determine the location of hydrogen atoms by the present characterization techniques [3, 20]. Note that, for modern advanced structured materials, a complex microstructure, e.g., consisting of multiple phases and precipitates, could result in the multiple dimensions of the complexity of HE mechanisms [21]. Keep all this in mind, the interpretation of the deformation microstructures with hydrogen charging via post-mortem analyses of fracture surfaces can be misleading and the derived mechanisms could be questionable. To clarify the associated mechanisms, more attempts at the in situ observation of hydrogen-microstructure interaction are needed.

As dislocation is the most important plasticity carrier for metallic materials, a comprehensive investigation of hydrogen-dislocation interaction mechanisms is thus of great importance to help us understand the observed HE phenomenon. Although in situ environmental TEM has been performed to demonstrate the dislocation structure evolution [9], the combination of serious stress relaxation and strong surface effect, raised due to the thin foils used for TEM, renders it difficult to validate the hydrogen-dislocation interaction mechanism and to extend it to bulk materials. To overcome these challenges, an investigation of the interplay between dislocations and hydrogen should be performed

more directly. Owing to the high-quality SEM instruments that provide concurrent small beam convergence, high current density, and small beam diameter [22], the ECCI technique can be used for direct observation of crystal lattice defects, e.g., dislocations, SFs, and GBs within bulk samples. The basic mechanism of ECCI for defects observation is related to the channeling condition [23]. To obtain optimum contrast, the so-called two-beam diffraction condition is achieved, where only one set of lattice planes is tilted into the Bragg condition. Under this condition, the perfect crystal is illuminated in the channeling conditions, which will show low intensity in the backscattered diffraction detector (BSD), while for the crystal associated with lattice defects, the atom columns there are shifted away from the exact Bragg condition, resulting in strong backscattering and thus a strong contrast difference with the surrounding perfect crystal [22]. Here, ECCI was applied to observe dislocation structure evolution after hydrogen adsorption and desorption.

2 Experimental

The chemical composition of the selected material is Fe-27.81Mn-0.3C (in wt%). Detailed information on material preparation and heat treatment can be found elsewhere [16, 24]. After heat treatment, the material showed a fully face-centered cubic (fcc) structure with an average grain size of 17.8 μm . The hydrogen adsorption and desorption processes are demonstrated in Fig. 1a1–a3. The light blue dots represent hydrogen atoms. Note that the hydrogen distribution could be extremely nonuniform, which depends on the microstructural heterogeneity and will be discussed in the following section in detail. Tensile specimens were prepared by electric discharge machining (EDM), which were polished with SiC grinding papers from 220 to 1000 grit, then polished by 1 μm diamond suspension for 15 min, and a final polishing with 50 nm colloidal suspension of SiO₂ (OPS) for 20 min. Before deformation, hydrogen pre-charging was performed in a 0.05 M H₂SO₄ aqueous solution containing 1.4 g/L CH₄N₂S as hydrogen recombination poison with a cathodic density of 1 mA/cm² at ambient temperature for 120 h, as schematically demonstrated in Fig. 1b. After hydrogen charging, the sample was slightly polished with OPS for around 1 min to maintain high surface quality for characterization. Thereafter, the sample was immediately deformed to a global strain of 2% and then reloaded for stress relaxation (Fig. 1a2). ECCI observations of the deformed microstructures were performed right after the sample was placed in a scanning electron microscope (SEM) chamber. After that, the sample was kept in the chamber with a high vacuum for 10 h without any further operation, to avoid the effect of external stress on dislocation movement. It can be deduced that hydrogen could desorb from the sample surface during vacuum aging. To prove this, thermal desorption mass

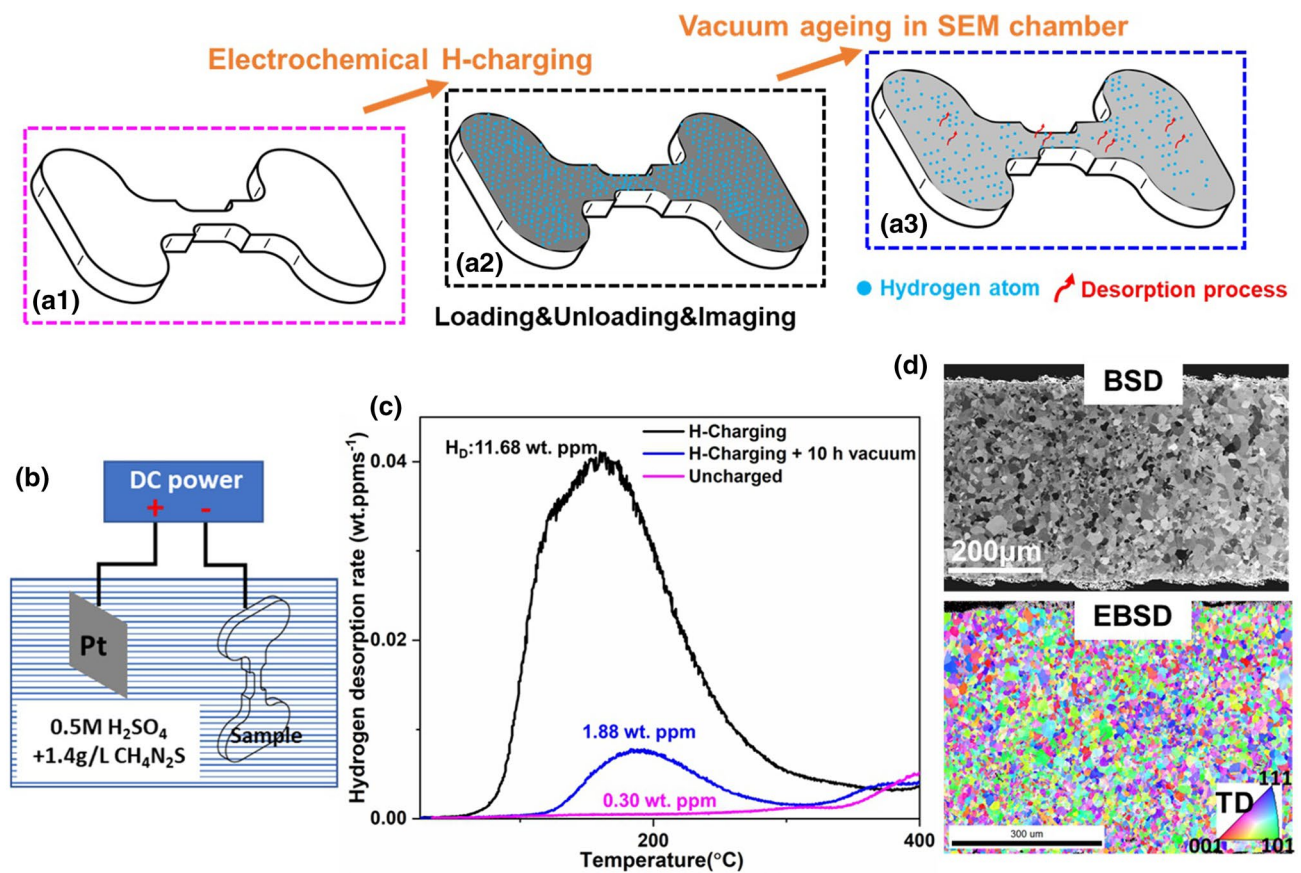


Fig. 1 Illustration of experimental procedures: **a1–a3** schematic of hydrogen adsorption and desorption processes, **b** electrochemical hydrogen charging set-up, **c** thermal desorption rate curves showing the diffusible hydrogen contents for samples under different conditions, **d** BSD and EBSD overviews of the deformation region of interest. BSD: backscattered diffraction. EBSD: electron backscattered diffraction

spectrometry (TDS) was carried out from room temperature (RT) to 800 °C to measure the hydrogen contents of the sample under different conditions. Note that the content of diffusible hydrogen was calculated by the cumulatively desorbed hydrogen from RT to 300 °C. As shown in Fig. 1c, compared to the un-charged sample, about 11.7 wt. ppm of diffusible hydrogen was charged into the sample after 120 h hydrogen charging (also reported in a previous study [16]). However, the hydrogen content decreased significantly (only 1.88 wt. ppm left) after being exposed to a vacuum for 10 h. Backscattered electron (BSE)/ECCI and electron backscattered diffraction (EBSD) were performed to observe the dislocation structure and grain orientation, as illustrated in Fig. 1d. EBSD scan was carried out using an EDAX/TSL Hikari camera with TSL OIM data collection software in Zeiss XB1540 with an accelerating voltage of 15 kV and a step size of 0.5 μm. BSE and ECCI were performed using a Zeiss Merlin SEM with an accelerating voltage of 30 kV and a working distance of 7 mm. A semiconductor four-quadrant BSE detector with a diameter of 10 mm was used. The channeling condition for performing ECCI was achieved based on a simulated electron channeling pattern (ECP) using the software tools for orientation

determination and crystallographic analysis (TOCA) [25]. Before ECCI observation at low tilts, the sample was positioned at a high tilt angle (like 70°) for EBSD measurements of the region of interests. Thereafter, the orientation information based on EBSD measurement was entered into TOCA software for ECP simulation. With the assistance of TOCA, the stage tilts and rotations needed to bring a crystal into optimum channeling condition were given. It should be mentioned that due to the accuracy limitations of EBSD and the uncertainty of the SEM stage control, a discrepancy between the TOCA-predicted orientation and the real channeling orientation could exist. To decrease this error, orientation calibration has been performed. Detailed information on the calibration process can be found elsewhere [22, 24].

3 Results

Typical results are displayed in Fig. 2 to compare the dislocation patterns of the un-charged and hydrogen-charged samples. From Fig. 2a, it can be seen that a very low dislocation density ($\sim 10^{12}/\text{m}^2$, estimated by counting the number of

dislocation/surface intersections) appears in the un-charged sample before deformation. Similar dislocation density is also observed after hydrogen charging (Fig. 2b), which indicates that no obvious defects were introduced during the charging process. To elucidate the effect of hydrogen on deformation microstructure, grains with similar tensile direction (TD// [212]) were selected from both un-charged and hydrogen-charged samples at a global strain amplitude of 2%. The channeling conditions (g vectors) of selected grains were obtained based on the simulated ECP by TOCA. For example, the white cross in the inlet of Fig. 2c indicates the present channeling condition of the observed grain. As shown in Fig. 2c, perfect dislocations distribute along slip traces in the un-charged sample. SFs are rarely observed in the un-charged sample due to the relatively high SFE (27 mJ/m^2 [16]). In contrast, emission of partial dislocations

with extended SFs from GBs is frequently observed in the hydrogen-charged sample, as shown in Fig. 2d. Some of the SFs extend up to hundreds of nanometers through the whole grain with the leading partials being trapped on the opposite GBs.

As indicated by TDS results, after vacuum aging in the SEM chamber for 10 h, most of the hydrogen atoms desorb out of the sample. The microstructure evolutions after vacuum aging are given in Figs. 3 and 4. ECC images in Figs. 3a1, 4a1, b1 show deformation microstructures of the hydrogen-charged sample before vacuum aging, which were taken within 30 min after the sample was placed in the SEM chamber. Microstructures of the corresponding grains after vacuum aging were displayed in Figs. 3a2, 4a2, b2. By comparing Fig. 3a1 and a2, it can be seen that the split distances of SFs decrease after hydrogen desorption. In detail,

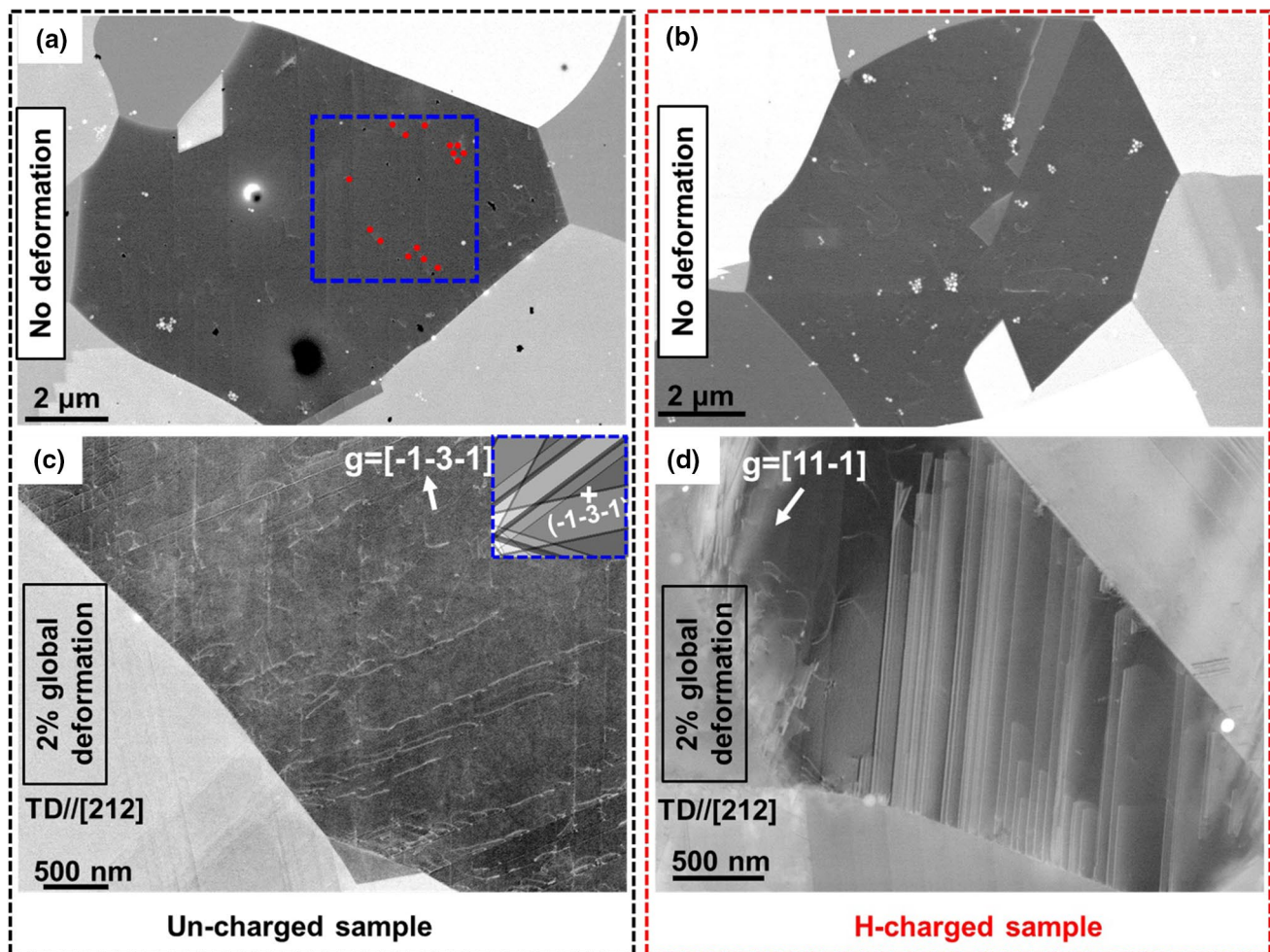


Fig. 2 ECC images displaying the dislocation configurations: **a** un-charged sample and **b** hydrogen-charged before deformation; **c** un-charged sample and **d** hydrogen-charged sample at a global strain amplitude of 2%. An example showing the estimation process of dislocation density from ECC images is displayed in **a**. The intersections of individual dislocations with the surface are marked by red dots. Dislocations density is obtained by counting the total number of the red dots divided by the area of blue rectangle. Inset in **c** showing the simulated electron channeling pattern. TD: tensile direction

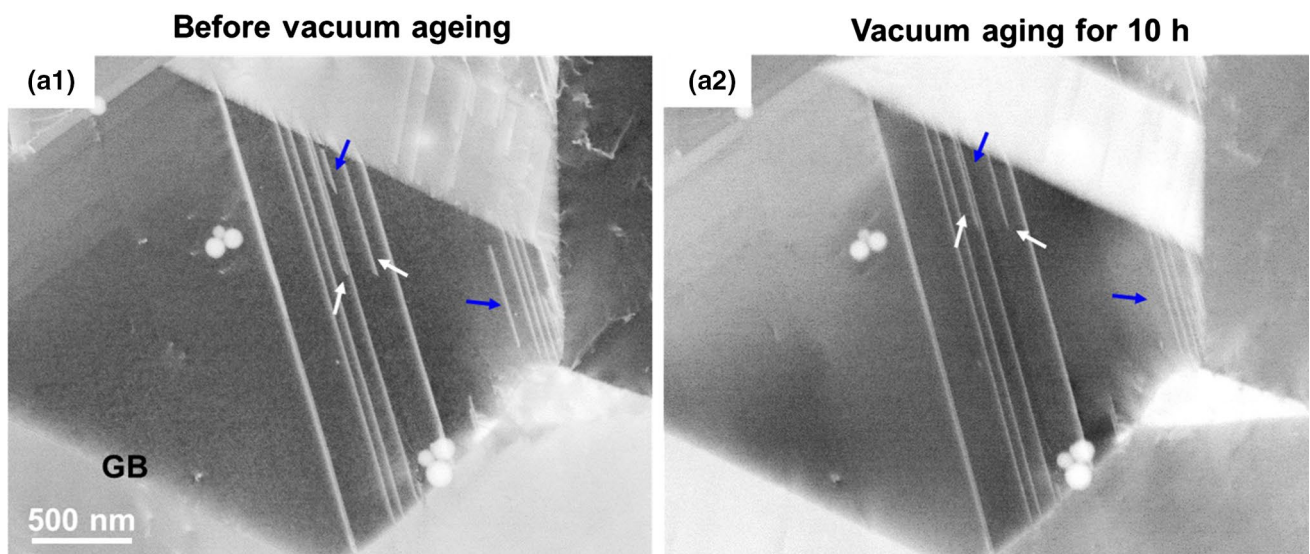


Fig. 3 Evolution of stacking fault configurations in the deformed sample **a1** before and **a2** after vacuum aging (hydrogen desorption)

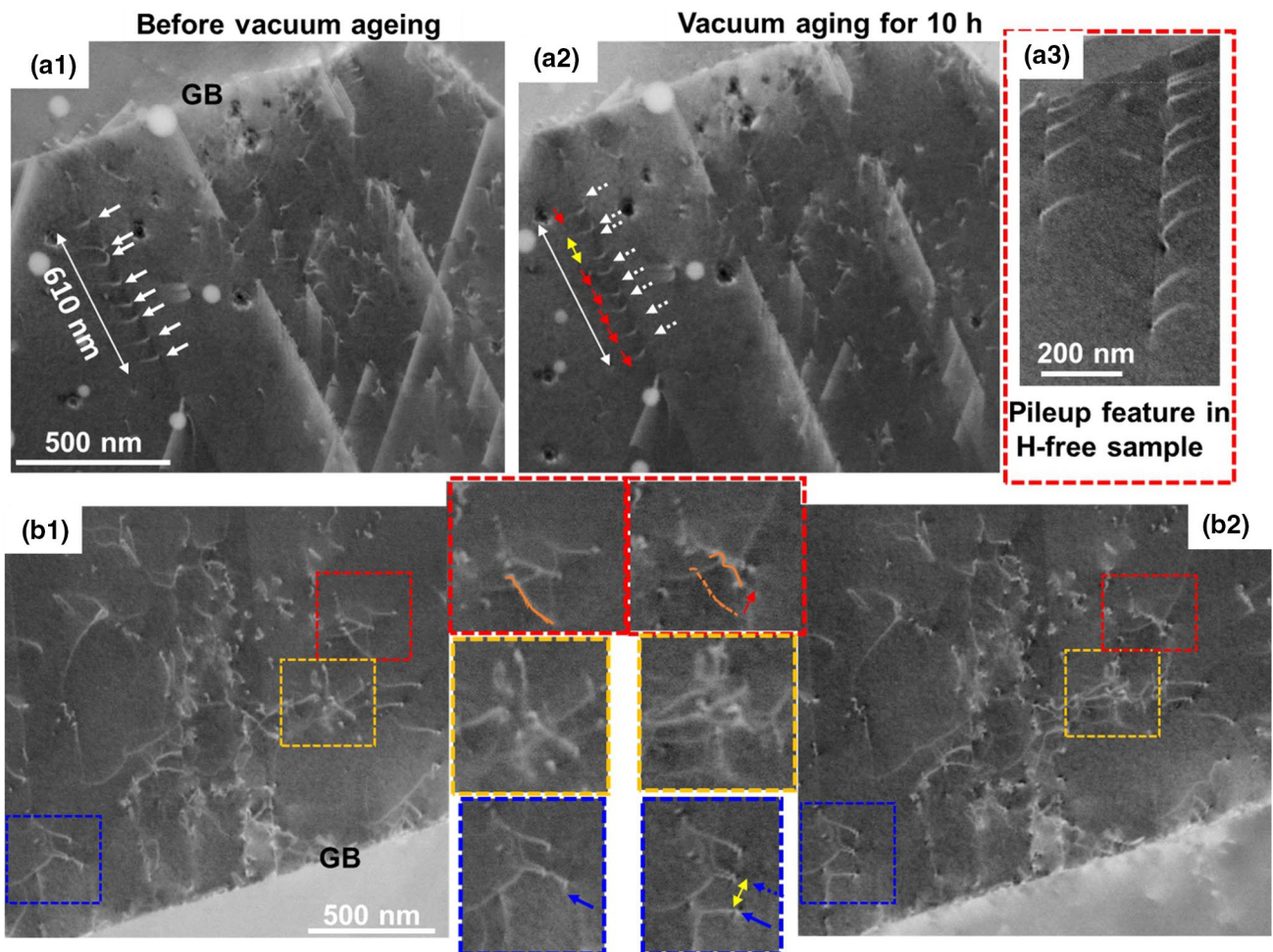


Fig. 4 Evolution of the dislocation configurations in the deformed sample **a1**, **b1** before vacuum aging and **a2**, **b2** after vacuum aging (hydrogen desorption). Enlarged views of interested regions in **b1**, **b2** displayed in rectangles with corresponding colors. **a3** An example showing a typical pile-up feature in the hydrogen-free sample. GB: grain boundary

SFs with two free bounding partials, e.g., those highlighted by blue arrows in Fig. 3a1, disappear after 10 h of vacuum aging. SFs with one free partial, e.g., those marked by white arrows in Fig. 3a1, are found to shrink toward the GBs. In contrast, SFs with both partials being trapped by GBs remain stable after vacuum aging.

Similar observations regarding SF shrinkage can also be found in Fig. 4a1, a2. Besides, the movement of perfect dislocations after hydrogen desorption is observed. As shown in Fig. 4a1, dislocations are found to arrange in a planar array piling up to a GB, as highlighted by white arrows. Note that the typical feature of pile-ups normally shows an increasing spacing between successive dislocations away from the GB, an example is given in Fig. 4a3. In contrast, dislocation spacing in the hydrogen-charged sample shows almost constant values (within the range between 80 and 90 nm) in the observed planar array. For clarity, the positions of dislocations before vacuum aging are marked as white dashed arrows in the ECC image after vacuum aging (Fig. 4a2). Surprisingly, the sequenced dislocations are found to move away from GB at a scale of tens of nanometers after hydrogen desorption, as highlighted by red arrows in Fig. 4a2, apart from the tangled dislocations, which repel each other (marked by the yellow arrow in Fig. 4a2). For clarify, enlarged views of interested regions in Fig. 4b1, b2 are displayed, highlighted by rectangles with corresponding colors. It can be seen that dislocation repulsion is frequently observed in the studied material, e.g., the dislocations marked by the blue arrow in the blue rectangles of Fig. 4b1, b2. Nevertheless, dislocation attraction is also observed after hydrogen desorption, like the regions highlighted by red and gold dashed rectangles. Owing to the convenience of ECCI, statistical analyses of deformation microstructures after hydrogen charging and

hydrogen desorption have been performed, which ensure the generality of those observed dislocation activities, e.g., dislocation attraction, dislocation repulsion, and SF shrinkage.

4 Discussion

By analyzing deformation microstructures after hydrogen adsorption and desorption using ECCI, it can be revealed that hydrogen plays a complex role in dislocation behavior. For example, hydrogen desorption could result in dislocation attraction or repulsion in the same grain. This discrepancy is more likely to be due to the very inhomogeneous distribution of hydrogen and local residual stress, as schematically demonstrated in Fig. 5.

The formation of hydrogen-assisted SFs in the studied material was also reported in a previous study [16], which was ascribed to the Suzuki effect. As schematically demonstrated in Fig. 5a, segregation of hydrogen atoms to SFs (highlighted by blue arrows) is assumed to reduce the local SFE, which increases the dissociation width of the bounding partials. After vacuum aging, amounts of hydrogen atoms desorb out of the SFs (highlighted by red curved arrows), leading to a significant increase of the local SFE and, thus, a strong constriction force exerted on the bounding partials. Consequently, the bounding partials move back and the SFs shrink toward GB, as demonstrated in Fig. 5b. The observed SF evolution after hydrogen desorption further verifies the proposed Suzuki effect.

In this study, cathodic charging was performed, which was reported to generate a strong hydrogen concentration gradient from surface to center [26]. As estimated in a previous study, where the same electrochemical hydrogen charging

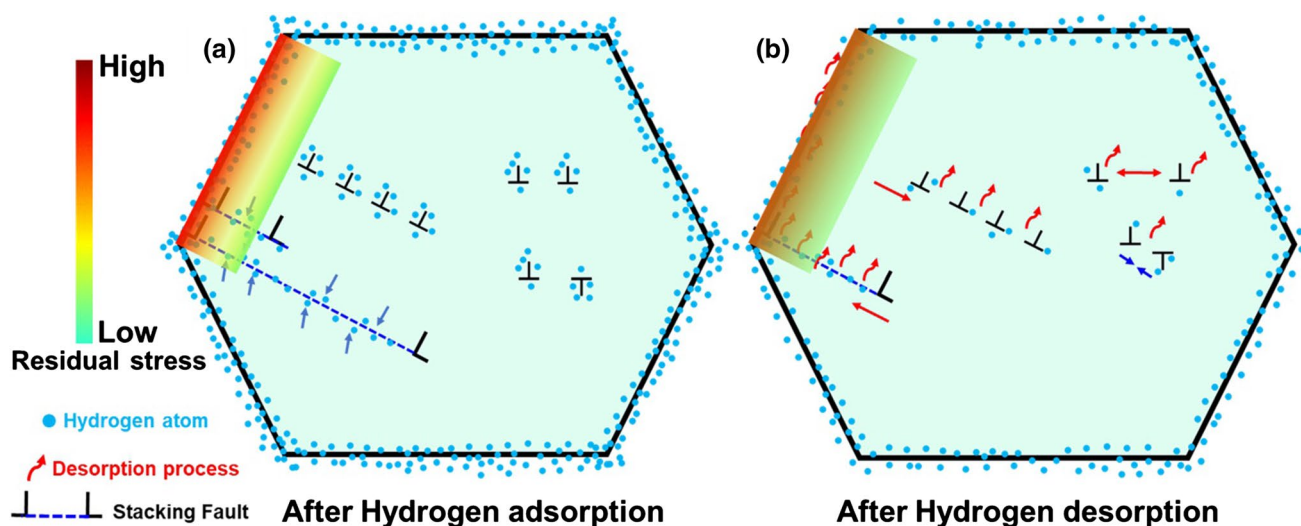


Fig. 5 Schematic illustration of the hydrogen-dislocation interaction mechanisms after **a** hydrogen adsorption and **b** hydrogen desorption

parameters were applied, the hydrogen content of the sample surface can reach around 60 wt. ppm [16]. Furthermore, the depth of the hydrogen-affected regions, estimated by post-mortem analysis of the fractured surface, is around 100 μm . Although slight OPS was performed (~ 1 min) on the sample after hydrogen charging, the removed depth is estimated to be less than 1 μm [27]. Therefore, the hydrogen level of the observed sample remains relatively high. As reported by Waldemar et al. [28], the hydrogen concentration on the sample surface was not homogeneous. In detail, vacancies and dislocations were dominant hydrogen trapping sites. Moreover, hydrogen segregations in crystal defects are also proposed in both experimental [3, 29] and simulation [5, 30] studies. Therefore, the hydrogen concentration within these defects is significantly higher than the estimated value (60 wt. ppm). As demonstrated in Fig. 5a, hydrogen atmospheres surrounding the dislocation core can shield the back stress exerted from the subsequent piled-up dislocations. Therefore, the spacings between planar dislocation arrays in the hydrogen-charged sample observed in this study show almost constant values.

Note that high hydrogen concentration near the sample surface could cause severe surface expansion. The heterogeneous distribution of hydrogen concentration can introduce a variety of local residual stress in a Fe–Mn-based high-entropy alloy, as proposed by Koyama et al. [5]. Similarly, reasonable speculation for the observed dislocation movement in this study could also be attributed to the heterogeneously distributed residual stresses. It was reported that hydrogen atoms prefer to segregate to random high angle GBs (RHAGBs) rather than dislocations [31]. It can be imagined that there exists a larger stress field near RHAGB, as schematically illustrated in Fig. 5a, b with the background colors of the rectangle overlaid on it. During vacuum aging, hydrogen atoms desorb more easily out from dislocation cores than from GBs, which was also reported in [5]. During this process, the shielding effect of the hydrogen atmosphere weakens while the long-range stress field near GB remains exists. Consequently, the planar dislocation arrays are repelled away from the GBs, as illustrated by the red arrow in Fig. 5b.

The stochasticity of dislocation movement, e.g., dislocation attraction or repulsion, after hydrogen desorption could be due to the difference in signs of dislocation Burgers vector. Figure 5b displays two simplified cases, i.e., edge dislocations with same and opposite Burgers vectors. After the vanishing of the shielding effect, dislocations with the same Burgers vector will repel each other, while those with opposite signs will attract each other [32]. Nonetheless, the underlying mechanisms for dislocation movement could be more complicated in the real case, which should take into consideration of GB types, dislocation types, hydrogen concentrations, local resolved shear stress, etc.

5 Conclusions

In this study, the dislocation structure evolution after hydrogen adsorption and desorption was investigated using ECCI, and some conclusions can be obtained as follows:

1. Hydrogen assists the formation of SFs in terms of the Suzuki effect, which is supported by both hydrogen adsorption and desorption results.
2. Hydrogen atmosphere surrounding dislocation cores plays a role in the observed constant dislocation spacing in planar pile-ups.
3. The required resolved shear stress for dislocation movement could be due to the local residual stress caused by hydrogen segregation.
4. The underlying hydrogen-dislocation interaction mechanisms are complicated, which leads to the discrepancy of dislocation activities even within the same materials due to the microstructural heterogeneity.

Acknowledgements This work was financially supported by the National Natural Science Foundation of China (No. 52101022) and the Shaanxi Province Natural Science Foundation (No. 2021JQ-080).

Declarations

Conflict of interest The authors state that there are no conflicts of interest to disclose.

References

- [1] A.J. Breen, L.T. Stephenson, B. Sun, Y. Li, O. Kasian, D. Raabe, M. Herbig, B. Gault, *Acta Mater.* **188**, 108 (2020)
- [2] M. Koyama, E. Akiyama, K. Tsuzaki, *Corros. Sci.* **54**, 1 (2012)
- [3] Y.S. Chen, H. Lu, J. Liang, A. Rosenthal, H. Liu, G. Sneddon, I. McCarroll, Z. Zhao, W. Li, A. Guo, J.M. Cairney, *Science* **367**, 5 (2020)
- [4] X. Li, X. Ma, J. Zhang, E. Akiyama, Y. Wang, X. Song, *Acta Metall. Sin. -Engl. Lett.* **33**, 759 (2020)
- [5] K. Motomich, M.T.M. Seyedeh, Y. Haoxue, K. Jinwoo, C.C. Benjamin, S.M.A. Seyed, L. Ju, C.T. Cemal, *Sci. Adv.* **6**, eaaz1187 (2020)
- [6] B. Sun, W. Lu, B. Gault, R. Ding, S.K. Makineni, D. Wan, C.H. Wu, H. Chen, D. Ponge, D. Raabe, *Nat. Mater.* **20**, 1629 (2021)
- [7] C.D. Baechem, *Metall. Trans.* **3**, 437 (1972)
- [8] D.S. Shih, I.M. Robertson, H.K. Birnbaum, *Acta Metall.* **36**, 111 (1988)
- [9] P.J. Ferreira, I.M. Robertson, H.K. Birnbaum, *Acta Mater.* **46**, 9 (1998)
- [10] P. Sofronis, I.M. Robertson, *Philos. Mag. A* **82**, 3405 (2002)
- [11] R.A. Oriani, *Acta Metall.* **18**, 11 (1970)
- [12] R. Kirchheim, *Scr. Mater.* **62**, 67 (2010)
- [13] J.D. Hermida, A. Roviglione, *Scr. Mater.* **39**, 1145 (1998)
- [14] M. Koyama, E. Akiyama, K. Tsuzaki, D. Raabe, *Acta Mater.* **61**, 4607 (2013)

- [15] X. Lu, D. Wang, D. Wan, X. Guo, R. Johnsen, *Acta Metall. Sin. -Engl. Lett.* (2022). <https://doi.org/10.1007/s40195-021-01370-7>
- [16] D. An, W. Krieger, S. Zaefferer, *Int. J. Plast.* **126**, 102625 (2020)
- [17] I.M. Robertson, P. Sofronis, A. Nagao, M.L. Martin, S. Wang, D.W. Gross, K.E. Nygren, *Metall. Mater. Trans. A* **46**, 2323 (2015)
- [18] M. Wang, E. Akiyama, K. Tsuzaki, *Corros. Sci.* **49**, 4081 (2007)
- [19] M. Koyama, S. Okazaki, T. Sawaguchi, K. Tsuzaki, *Metall. Mater. Trans. A* **47**, 2656 (2016)
- [20] H. Zhao, P. Chakraborty, D. Ponge, T. Hickel, B. Sun, C.H. Wu, B. Gault, D. Raabe, *Nature* **602**, 437 (2022)
- [21] B. Sun, D. Wang, X. Lu, D. Wan, D. Ponge, X. Zhang, *Acta Metall. Sin. -Engl. Lett.* **34**, 741 (2021)
- [22] S. Zaefferer, N.N. Elhami, *Acta Mater.* **75**, 20 (2014)
- [23] D.C. Joy, D.E. Newbury, D.L. Davidson, *J. Appl. Phys.* **53**, R81 (1982)
- [24] D. An, H. Zhao, B. Sun, S. Zaefferer, *Scr. Mater.* **186**, 341 (2020)
- [25] S. Zaefferer, *J. Appl. Crystallogr.* **33**, 10 (2000)
- [26] H. Luo, W. Lu, X. Fang, D. Ponge, Z. Li, D. Raabe, *Mater. Today* **21**, 1003 (2018)
- [27] D. An, T.A. Griffiths, P. Konijnenberg, S. Mandal, Z. Wang, S. Zaefferer, *Acta Mater.* **156**, 297 (2018)
- [28] W. Krieger, S.V. Merzlikin, A. Bashir, A. Szczepaniak, H. Springer, M. Rohwerder, *Acta Mater.* **144**, 235 (2018)
- [29] M. Koyama, D. Yamasaki, T. Nagashima, C.C. Tasan, K. Tsuzaki, *Scr. Mater.* **129**, 48 (2017)
- [30] J. Song, W.A. Curtin, *Acta Mater.* **68**, 61 (2014)
- [31] D. Xie, S. Li, M. Li, Z. Wang, P. Gumbsch, J. Sun, E. Ma, J. Li, Z. Shan, *Nat. Commun.* **7**, 13341 (2016)
- [32] D. An, S. Zaefferer, *Int. J. Plast.* **121**, 244 (2019)